Image analysis and modelling of the orientation of pores in a constrained film on a rigid substrate

*By C.S. Ni & John T.S. Irvine**

Corresponding author: email jtsi@st-andrews.ac.uk

School of Chemistry, University of St Andrews, Fife KY16 9ST, Scotland

Abstract

The nature of porosity in functional materials is often a critical parameter in determining their functionality e.g. in structure materials and fuel cell electrodes. Here we study the development of the anisotropy of porous yttria-stabilized zirconia (YSZ), focusing particularly upon the contribution of pore orientation to this anisotropy. Simulation from when the ink is deposited on the surface of a rigid substrate shows that plate-like pores are found tend to align along the transverse direction of the substrate. Cross-sectional image analysis of the pores from the attendant pores of YSZ particles or pore forming agent (PFA) matches with the simulated modelling when materials transport is insignificant in determining the shape of pores. The anisotropy created in the densification stage is separated from that in the green body by analysing the image of porous structures formed with spherical glassy carbon which is unable to contribute to anisotropy during green state processing.

Keywords: constrained sintering, texturing, YSZ, porous ceramic.

Introduction

Porous ceramics are of significant interest in many fields due to their wide range of applications in energy-conversion and piezoelectric materials, biomaterials, catalyst supports and infiltration membranes[1]. Among the methods used to prepare porous ceramics, screen printing is a low-cost method that is scalable and well-suited for the fabrication of thick film (10 - 50 μm) on rigid substrate. For example, pre-sintered porous YSZ scaffold via screen printing can be infiltrated with conductive perovskite to prepare highly active electrodes for solid oxide fuel cell[2,3]. The addition of pyrolyzable pore former is a simpler but more effective way of producing pores in ceramic sintered at high sintering temperature for better connectivity and/or bridging between the components, compared to the alternative partial-sintering method. Graphite is a popular choice as pore forming agent (PFA) because of the vast availability and compatibility with the organic solvent, but its two-dimensional shape causes the anisotropy of the ceramics.

The preferred orientation (or texturing) is of great interest because it is common in ceramics and has significant influence on physical properties such as strength[4], mass transport[5,6], electrical conductivity[7], and optical property[8,9]. To be specific, the shape and array of pores in the electrode of a solid oxide fuel cell dictates the tortuosity of the gas permeation[5] and the distribution of the infiltrated phases[10,11]. However, the cause of anisotropy of the pores comes from two major sources which tend to cause orientations in perpendicular directions to each other. The non-uniform packing density of a green body prepared by tape casting and the anisotropy from the particles are thought to be important directors for the orientation[12,13,14,15,16]. For a green body fabricated using screen printing or tape casting, the particle rearrangement by capillary forces takes place when the solvent evaporates and the surface of slurry retracts to the substrate. This arrangement is able to change the orientated pores to a

direction more aligned to the in-plane direction. On the other hand, in the case of a screen printed film where no in-plane shrinkage is allowed in a continuum system, the orientation can also arise from the constrained sintering process of a screen-printed layer for dense ceramic; the pores align along the direction perpendicular to the film plane[17,18] owing to the uneven materials transport between the in-plane direction and its perpendicular direction. The anisotropy from the two sources is perpendicular to each other and causes the final texturing in the ceramic to be difficult to predict. As a result, a balance of the two reasons for anisotropy should be considered in the very screen printed porous ceramic on a rigid substrate.

In this work, image analysis and modelling based on the continuum assumption of the green body or ceramic film were used to study the microstructure orientations at different stages starting from the application of inks to the final sintered ceramic. Inks with graphite (plate-like in shape) or glassy carbon (spherical in shape) were used to detect the orientation evolution at different stages of sintering. Moreover, the two-dimensional images of anisotropic pores with varied pore size distributions were generated to study the relationship between the pores of two scales: small interstitial pores among ceramic particulates (~0.1 μm) to large pore former (~1 μm).

Experimental

Materials

Two types of 8 mol.% Y_2O_3-stabilised ZrO_2 (8-YSZ) were used in the ink making process, Unitec 8-YSZ 1-um and 2-um powder (denoted as Unitec 1-um and 2-um powder) both from UCM Advanced Ceramics GmbH, Laufenburg, Germany. The particle size analysis (PSA) of the two 8-YSZ powders was performed on a

Mastersizer 2000 particle size analyzer (Malvern Instruments LTD, Malvern, UK) after ball milling in an isopropanol solution containing 2 wt.% triton as surfactant for 24 h to simulate the de-agglomeration process during ink-making. The size distributions are shown in Figure 1 (a), and are consistent with the SEM images (Figure S1), i.e. the Unitec 1-um powder contains finer particles. The PSA data of 2-um powder show only one peak at ~1 μm, while those of 1-um powder exhibit two peaks at 0.1 μm and 0.8 μm. A pellet of 13 mm in diameter and 1 mm in thickness was obtained by pressing the powder under a uniaxial pressure of 149 MP and then its sinterability was measured via a dilatometer (DIL 402C, NETZSCH GmbH & Co. Holding KG, Germany) with a heating rate of 3 ^{o}C/min up to 1350 ^{o}C, as shown in Figure 1 (b). Results show that the Unitec 1-um powder started to sinter at 950 ^{o}C and the other would not sinter until the temperature reaches 1100 ^{o}C. The shrinkage of the pellets from Unitec 1-um powder is twice that from Unitec 2-um powder after dwelling for 3 h.

Sample preparation and image analysis

In the ink-making process, Hypermer KD-1 (Croda Inc. East Yorkshire, UK) was used as dispersant, and terpineol containing 5 wt. % Butvar Polyvinyl Butyral (PVB) as a vehicle. The pore former is graphite (325 mesh, Alfa Aesar, Lancashire, UK) or glassy carbon (Alfa Aesar, Lancashire, UK). The graphite is composed of aggregated plates with varied dimensions while the glassy-carbon particles are 10-20 μm spheres. A mixed powder containing the YSZ powder, and PFA (if any) was ball milled at 160 rpm for 24 h in a plastic bottle containing 36 1-cm diameter zirconia balls using acetone as solvent. Then the contents, except zirconia balls, were transferred to a beaker followed by the addition of vehicle. The acetone is allowed to evaporate while

stirring, resulting in a well-dispersed viscous ink. The recipes of the inks with or without PFAs are shown in table 1. The amount of PFAs is controlled to be small in order to avoid their possible interaction.

3.7 g 8-YSZ (HSY-8, DKKK, Osaka, Japan) powder was uniaxially pressed at a static pressure of 150 MPa and sintered at 1500 ^{o}C for 10 h to result in a dense pellet of 2-mm thickness and 2 cm in diameter. The screen printing process was performed using a computer-controlled machine (248 Dek Printing Machines, Shenzhen, China) and a 325-mesh screen and 2-mm printing gap were used for the thick layers. The squeegee was under a load of 60 kN and moves at a speed of 35 mm/min. The viscosities (Figure S2.) of the inks were measured with a programmable rheometer (Brookfield DV-III ultra, Middleboro, MA), and were quite similar to each other. The screen-printed pellets with inks 1, 2 and 4 were then sintered at 1320 ^{o}C for three hours using a heating ramp of 1 ^{o}C/min before 1000 ^{o}C and 3 ^{o}C/min afterwards with a cooling ramp of 3 ^{o}C/min. The pellet with ink 3 was sintered at 1100 ^{o}C for 3 hours with a heating ramp of 1 ^{o}C/min and cooling rate of 1 ^{o}C/min. The sintered samples were vacuum mounted in an epoxy, cut with a diamond saw and polished to 1-μm diamond polishing paste. The backscattered-electron images were taken on a Jeol 6700F to give highly contrasting images which were binarized by choose a threshold to separate the pores and ceramics and analyzed with ImageJ software (National Institute of Health, Bethesda, MD). The choice of threshold is verified with the porosity from the measurement of weight and thickness. The evaluation of particle orientation was accomplished by circumscribing a best-fit ellipse to every single particle, as demonstrated in reference 12. The angles of the particles are converted into the range 0-π/2. The particles with an area less than 0.01 μm^2 or 0.6 μm^2 for the image of ink

without PFA or with PFA respectively were not taken into account due to the difference in magnification of the images.

Modelling of the rearrangement of PFA/pore

The sintering properties of a ceramic are, to some extent, dependent on the local interaction between the particles and macroscopic properties (>1 μm)[19]. The use of continuum mechanics, which has been successfully applied to the analysis of compaction of porous bodies, is extended to the whole process starting from the point when the slurry is deposited on the rigid substrate, as demonstrated in Figure 2. L_0 is the thickness of the inks on the surface of the substrate (initial state) and L_1 is the thickness when the sintering is about to start after the drying process and burning off the organics and pore former. After the sintering at the final temperature, the thickness of the film becomes L_2. In the whole process, a plate-like graphite/attendant pore is going to rotate and align toward the surface of the substrate as shown in the magnified area in Figure 2, where a continuum of the system is assumed. Because the ink will be confined in the compartment of the screen, and the squeegee and mesh will confine the move of liquid in the depositing process, and therefore the effect of Marangoni convection could be diminished in screen printing. X-axis is the reference axis for the angle of particles. The plate-like graphite burns off at a temperature below 900 ^{o}C to produce pores of the same shape, so the plate-like pore former is assumed to be interchangeable with the pores in the modelling process. The interaction among pore formers is also neglected since the amount of PFA is small. Because of the rigid substrate, the reaction or shrinkage in the in-plan direction is negligible and the relation between θ_0 and θ_1 can be represented in the equation:

$\theta_1 = arctan(L_f/L_0 * tan(\theta_0))$ (1)

where L_f is the thickness of the film in the range of [L_0, L_1]; θ_0 and θ_1 represent the angle of the graphite and pore in relation with the x axis. The shrinkage of film, δ, is determined by equation:

$\delta = 1 - L_f/L_0$ (2)

Specifically, the shrinkage in stage I, τ, and the shrinkage at stage II, κ, are defined as

$\tau = 1 - L_1/L_0$ (3)

$\kappa = 1 - L_2/L_1$ (4)

It should be noted that before the removal of graphite, the length of graphite that is represented by the cross-section of plate-like graphite on the plane of interest varies with the rotation process in the modeling, but this is more applicable to the situation of pores after the burning of PFA.

One thousand graphite particles of normalized length distribution were randomly generated on a 50 μm by 50 μm area. The linear angle distribution, Figure 3 (a), indicates a random distribution of the pore former in the initial stage, suggesting that 1000 pore formers/pores are sufficient to represent a random system. The pore size distribution of two sets of pore formers / pores is indicated in Figure 3 (b), denoted as PS_1 and PS_2. The pore sizes cover about 5 decades. The anisotropic image is intensified as δ increase from 0 to 0.9 in the slurry based system. Patwardhan[20] studied the pore anisotropy of tape-cast ceramic in y direction, and found that low-

solid-loading slurry produces more intense anisotropy, and this could be understood by a smaller δ value for a film with less solvent. Actually, this model also indicates that a looser-packing system is more prone to produce anisotropy given the same final density, similar to the study of Zainuddin[21]. In this study, the image of the film at different shrinkages, δ, is shown in Figure 4, where the length of each particle in (a) is elongated by a factor of 5, as shown in (b). The image was then compressed to simulate the drying process and constrained sintering in the y-axis without considering the variation of pores by transport process. A tape-cast film with coarser powders is found to be more orientated than that with finer powders of similar geometry[23]. The image simulation indicates that only the large pores are obvious in the image. The comparison of these two images also suggests that image analysis at an inappropriate magnification is misleading sometimes because of the capacity of the information in the images.

The cumulative percentage of orientation profile at different stage of sintering is showing in Figure 5 if equation 1 is used to predict the angle change from a random distribution system. The cumulative probability equation is

$$\Gamma=(2/\pi)\arctan((1-\delta)^{-1}\tan(\theta)) \qquad (5)$$

where Γ is the cumulative probability of the particles with an angle of θ.

The percentage of the particles within π/4 is used to index the anisotropy of the film[22,23], even though Guillon et al. [17,24] and Mucke et al. [25] proposed different parameters to indicate the pore orientation. For instance, when δ is 0.9, 90 % of the particles have an angle less than π/4. In order to single out the anisotropy induced

during the sintering process, the shrinkage of the stage II, κ, couple with the shrinkage in stage *I*, τ, is used to predict the orientation and the result can be represented in the formula:

$$\Gamma=(2/\pi)\arctan((1-\kappa)^{-1}(1-\tau)^{-1}\tan(\theta)) \qquad (6)$$

When τ equals zero, the orientation of particles is governed totally by the sintering process. The one dimensional shrinkage value κ is different from the parameter measured from the dilatometery data because the constrained densification is greatly retarded compared to free sintering[26,27]. However, if there is a massive transport of materials between the ceramic particles, the orientation profile will deviate completely from the prediction above as analyzed below.

Results and discussion

Image analysis of the anisotropy from sintering of the film without PFA

The cross-sectional images of the two films from Unitec 1-um and 2-um powder are shown in Figure 6 (a) and (b) and the corresponding binary images of the film are shown accordingly in (c) and (d). The average thickness of film from Unitec 1-um and 2-um is to be 24.9 μm and 31.5 μm, respectively, by analyzing five images at this magnification. Images at higher-magnification images (Figure S3) are analyzed for the porosities of films, and the average porosities from five images are 29 % and 40 % for the film from 1 um and 2 um powder, respectively. We also used the weight of the porous structure and the thickness to calculate the density, and the porosities are 28% and 38%, for the film from 1 um and 2 um powder, which are consistent with the data

from image analysis. Based on the conservation of mass of the ceramic in the porous structure and ink, the thickness of wet ink containing vehicle L_0 can be calculated:

$$L_0=L_f(1-\phi)/V_c \qquad (7)$$

ϕ is the porosity of the film and V_c is the volume fraction of the ceramic in the ink. Because the organics and PFA would be burn off below 450 [28] and 900 ^oC [29], respectively, this equation is valid at temperature above 450 and 900 ^oC for the sample without and with PFA.

In combination with equation 2, equation 7 gives

$$\delta= 1- V_c/(1-\phi) \qquad (8)$$

If the V_c value for the ink in table 1 is used, the shrinkage of ink with Unitec 1-um and 2-um should be 0.58 and 0.50, respectively, if the porosity from image analysis is used. The cumulative percentage of the diameter and angle of the pores are presented in Figure 7 (a) and (b). The pore size covers less than two decades, peaking at 0.25 μm and 0.32 μm for the ink with Unitec 1-um and 2-um powder, respectively, in the same order of the grain size measured by PSA, though the 2-D image analysis cannot represent the 3-D pore size very precisely. The asymmetry and narrow range of pore size distribution comparing to the simulation may be explained by the cut-off length of particles for counting or the sintering process that causes the disappearance of finer pores[18]. If the anisotropy of the ceramic powders and their attendant pores are rotating with the contraction of the films, the anisotropy of the pores should follow equation 5. However, the percentage of the particles with $\pi/4$ is less than 50% meaning the particles tend to be perpendicular to the substrate, in contrast to the prediction in

Figure 5, considering the δ value. Unitec 1-um powder tends to produce a more orientated microstructure with lower porosity then Unitec 2-um powder does, in agreement with the dilatometry curves, therefore we can conclude that the anisotropy is intensified by the degree of sintering that can be determined from the dilatometry. This trend coincides with the experimental result of Guillon et al.[17] but contradicts that of Wang et al.[18]. According to the simulation of Wang et al.[18] and Cannon et al.[30,31], the anisotropy caused by the faster in-plane grain diffusion with respect to grain boundary causes the spheroidization of the pores; anisotropy was found to increase then decrease along with the densification process[30]. The ultra-fine powder in the bi-model Unitec 1-um powder is beneficial in promoting the grain boundary diffusion in the sintering process, which explains the higher degree of anisotropy of the film from Unitec 1-um powder. The diffusion of the materials through the grain boundary in the densification process has significant influence on the pore shape in the attendant pores, but the possible initial in-plane anisotropy cannot be excluded.

Image analysis of the constrained film with plate-like pore former.

Although the anisotropy is affected by the substrate and densification process, in-plane anisotropy of $BaLa_4Ti_4O_{15}$ without PFA at the initial stage of sintering was also reported[32]. To study the anisotropy in stage I immediately after the densification process even started the ink with pore former (ink 3) was fired at 1100 ^oC when δ is equal to τ, and the cross-sectional image is shown in Figure 8 (a). The microstructure could be considered as the initial sintering stage, given the dilatometry data provided in Figure 1 (b). This image is dominated by long pores aligning along the x-axis, similar to the image in Figure 4, but more information about the pore size and orientation profile can be obtained with image analysis. The binarized image is

procured by choosing a threshold to separate the pores and ceramics, as shown in Figure 8 (b), with a porosity of 56.4%. The despeckling was used to delete the very fine pores (area < 0.6 μm^2) and a white line to separate some of the overlapping large pores manually for better analysis (Figure 8 (c))[23]. The Feret diameter was employed to evaluate the length of these extremely elongated pores and the discrete frequency profile is plotted in Figure 9 (a). The pore size is peaking at 1.18 μm, and contains a significant fraction of pores around 10 μm. Although the comparison of the distribution in Figure 7(a) and Figure 9 (a) shows an overlap in the range of 0.5-2 μm, but the attendant pores of the ceramic powder at 1100 ^oC should be much smaller than those at 1300 ^oC due to the diminishing of fine pores and growth of big pores. The profile of the distribution and the best-fitting curve with a parameter τ_s=0.64 is shown in Figure 9 (b). The τ value and was calculated to be τ_c=0.66 in equation 8 using the measured porosity and V_c in table 1. The good match between τ_s and the calculated τ_c indicates that the orientation profile is independent of the pore size distribution for the larger pores. An image with a τ value of 0.66 is provided using the same length profile of pores shown in Figure 9 (c). We can see that Figure 9(c) is quite similar to Figure 8 (c) in the anisotropy. The direct observation of the attendant pores at the starting temperature of sintering may be one way to detect the anisotropy at stage I, but the poor mechanical property and small size of the pores makes the result unreliable and difficult to analyze.

Image analysis of the constrained film with spherical pore former

Figure 10(a) shows the image from the ink with glassy carbon (ink 4) fired at 1100 ^oC for 3 hours, showing round pores resulted from the vestige of glassy carbon. Each

pore contains an inner shell separated from the porous YSZ matrix and this could be explained by the contraction of the glassy carbon coated with YSZ powder in the heating process[33]. However, after sintered at 1320 ^{o}C, the pores from glassy carbon compressed in y-axis direction to form ellipses as shown in Figure 10 (b), in contrast to pores from spherical particles in a free sintering system where no anisotropy was observed[34,35]. Albano et al.[33] found a good match between the shape of pore former in the green tape of tape casting and that of pores formed after being freely sintered. Because glassy carbon particles are spherical, the rotation in stage I does not exert any orientation in the green body of the film in stage I at the length scale of glassy carbon, ie, the anisotropy is attributed totally to the constrained sintering process. Due to the large length scale of pores from glassy carbon particles, the anisotropy from the diffusion is negligible in determining the shape of glassy carbon. Figure 11 shows the ratio of the Feret length of the pores in y axis direction in comparison to that in x axis, denoted as $R_{y/x}$. The pores in contact with the edge of the image are not included either. Most of the pores can be chosen to indicate the shrinkage because a continuous film of certain thickness is uniformly stressed except for those on the edge of the film where the pores show better densification[36]. We can observe the scattering of the $R_{y/x}$ values, indicating that some pores are not suited for demonstrating the anisotropy in this stage than the others. The overlapping between pores, the crack that appeared at high temperature sintering and the tilting owing to the unbalance force around each pore will affect the image analysis process. For film sintered at 1100 ^{o}C, the Feret lengths in x and y direction of the pores are similar to each other, since Ry/x is equal to 1.04. The $R_{y/x}$ is only 0.69 for the pores sintered at 1320 ^{o}C, indicating that the sintering from 1100 ^{o}C to 1320 ^{o}C causes a shrinkage of 0.31 in y direction, i.e, $\kappa=0.31$. If the same density is conserved, this linear κ value of 31 % corresponds to a

shrinkage value of 11.6 % in a 3-D shrinkage, which is slightly lower than the shrinkage measured from dilatometry at 1320 ^{o}C, ca. 15 %. For a system containing plate-like pores sintered at elevated temperature to the final state, the κ and τ should contribute together to enhance the anisotropy as calculated in Figure 5. However, the real situation is more complex because the difference in coordination number may result in change in the morphology of the pores [37], transport that causes the disappearance or growth of pores[18] and the defect evolution in the constrained film[38].

Conclusion

Two stages of orientation process are identified in this work without considering the transport of materials: the in-plane alignment caused by the confinement of the film in the forming of green body and the constrained sintering process. If the pores are in the scale of particles, ~0.1 μm, the uneven material transport will alter the shape of the pores to a direction normal to the substrate. On the contrary, for the pores from PFA on the scale between 1 and 10 μm, the effect of materials transport is negligible to the anisotropy. The image simulation offers more information that could be neglected in the real image analysis process, and a comparison of these parameters suggests that the anisotropy in the porous ceramic just before sintering is independent of pore size.

Acknowledgement

We thank EPSRC and ONR for funding and UCM for providing the ceramic powder.

Captions of Figures

Figure 1. (a) Particle size analysis of the Unitec 1-um and 2-um powder after ball milling for 24 h in isopropanol containing 2 wt.% triton. (b) Dilatometry of the pellets from two powders pressed under 149 MP.

Figure 2. Schematics of the thickness of the deposited film and the orientation of the pore/PFA at different stages. The axes are shown in the image to in indicate x- and y-direction. X-axis is the reference axis for the angle of particles.

Figure 3. (a) Cumulative angle distribution of the particles in the simulation work; (b) discrete pore size fraction of the 2D pores/PFAs used in the modelling, PS_1 is 4 times larger than PS_2.

Figure 4. Image evolution with pores/PFAs of random angle distribution at different shrinkage values. The length of the pore/PFAs in figure (a) and (b) is PS_1 and PS_2, respectively. The size of the original image when $\delta=0$ is 50μm x 50 μm. The width of images for the simulation of shrinkage, the width of image is 50 μm and the height change to $(1-\delta)$ x 50 μm by pressing the image from the top to the bottom. The insert image when $\delta=0.9$ are the zoom-ins of the area in the ellipses.

Figure 5. Statistics of the angle of the particles at different shrinkage in terms of δ values.

Figure 6. Back-scattered images of the film sintered at 1320 ^{o}C with ink containing Unitec 1-um (a) and 2-um (b) YSZ powder: (c) and (d) is the respective binarized image for calculation of porosity, pore orientation and pore size.

Figure 7. Pore size distribution (a) and cumulative fraction (b) of the constrained film from Unitec 1-um and 2- um YSZ powder as shown in Figure 6.

Figure 8. (a) back-scattered image of the film sintered at 1100 ^{o}C with the ink containing YSZ and graphite; (b) binarized image for measurement of porosity and (c) despeckled image for measurement of pore size and orientation. The scale bars represent 20 μm.

Figure 9. (a) Pore size distribution and (b) cumulative fraction of the pores at different angle. (c) is an image with the length profile of lines shown in (a) using the angle distribution when τ is 0.66.

Figure 10. Back-scattered images of the film sintered at 1100 ^{o}C (a) and 1320 ^{o}C (b) from the ink containing YSZ and glassy carbon. The length of scale bar is 10 μm.

Figure 11 the $R_{y/x}$ values for the pores from glassy carbon after a sintering at 1100 ^{o}C and 1320 ^{o}C. The straight line in each group of data shows the average value and the rectangle shows the standard deviation.

Caption of table

Table 1. Recipes of the inks with and without pore forming agent (PFA)

Reference

1 S. Somiya, F. Aldinger, N. Claussen, R.M. Spriggs, K. Uchino, K. Koumoto and M. Kaneno, Handbook of Advanced Ceramics. Volume II: Processing and Their Applications. Academic Press, Oxford, 2003.

[2] J. Chen, F. Liang, D. Yan, J. Pu, B. Chi, S. P. Jiang, and L. Jian, "Performance of Large-scale Anode-supported Solid Oxide Fuel Cells with Impregnated $La_{0.6}Sr_{0.4}Co_{0.2}Fe_{0.8}O_{3-\delta}$ $+Y_2O_3$ Stabilized ZrO_2 Composite Cathodes," *J. Power Sources,***195**[16] 5201-05 (2010).

[3] C. S. Ni, J. Vohs, R. J. Gorte, andJ. T. S. Irvine, "Fabrication and Characterisation of a Large-Area Solid Oxide Fuel Cell Based on Dual Tape Cast YSZ Electrode Skeleton Supported YSZ Electrolyte with Vanadate and Ferrite Perovskite- Impregnated Anode and Cathode," *J. Mater. Chem. A,***2** 19150-55 (2014).

[4] T. Ohji, "Microstructural Design and Mechanical Properties of Porous Silicon Nitride Ceramics," *Mater. Sci. Eng.: A,***498**[1–2] 5-11 (2008).

[5] J. R. Wilson, W. Kobsiriphat, R. Mendoza, H.-Y. Chen, J. M. Hiller, D. J. Miller, K. Thornton, P. W. Voorhees, S. B. Adler, and S. A. Barnett, "Three-dimensional Reconstruction of a Solid-oxide-fuel-cell Anode," *Nat. Mater.*,**5**[7] 541-44 (2006).

[6] S. W. Sofie, "Fabrication of Functionally Graded and Aligned Porosity in Thin Ceramic Substrates with the Novel Freeze-tape-casting Process," *J. Am. Ceram. Soc.*,**90**[7] 2024-31 (2007).

[7] J. Mizusaki, K. Waragai, S. Tsuchiya, H. Tagawa, Y. Arai, andY. Kuwayama, "Simple Mathematical Model for the Electrical Conductivity of Highly Porous Ceramics," *J. Am. Ceram. Soc.*,79[1] 109-13 (1996).

[8] J. Kim, J. Peretti, K. Lahlil, J.-P. Boilot, and T. Gacoin, "Optically Anisotropic Thin Films by Shear-oriented Assembly of Colloidal Nanorods," *Adv. Mater. (Weinheim, Ger.),* Doi: 10.1002/Adma.201300594 (2013).

[9] A. D. Rey and M. M. Denn, "Dynamical Phenomena in Liquid-crystalline Materials," *Annu. Rev. Fluid Mech.*,**34**[1] 233-66 (2002).

[10] M. J. Zhi, N. Mariani, R. Gemmen, K. Gerdes, and N. Q. Wu, "Nanofiber Scaffold for Cathode of Solid Oxide Fuel Cell," *Energy Environ. Sci.*,**4**[2] 417-20 (2011).

[11] C.S. Ni, M. Cassidy and J. T. S. Irvine, " Image Analysis of the Porous Yttria-Stabilized Zirconia (YSZ) Structure for the Impregnated Electrode of Solid Oxide Fuel Cell (SOFC)," to be published.

[12] J. L. Jones, B. J. Iverson, and K. J. Bowman, "Texture and Anisotropy of Polycrystalline Piezoelectrics," *J. Am. Ceram. Soc.*,**90**[8] 2297-314 (2007).

[13] A. Heunisch, A. Dellert, and A. Roosen, "Effect of Powder, Binder and Process Parameters on Anisotropic Shrinkage in Tape Cast Ceramic Products," *J. Eur. Ceram. Soc.*,**30**[16] 3397-406 (2010).

[14] F. V. Dimarcello, P. L. Key, and J. C. Williams, "Preferred Orientation in Al_2O_3 Substrates," *J. Am. Ceram. Soc.*,**55**[10] 509-14 (1972).

[15] S. Tanaka, Y. Kuwano, and K. Uematsu, "Packing Structure of Particles in a Green Compact and Its Influence on Sintering Deformation," *J. Am. Ceram. Soc.*,**90**[11] 3717-19 (2007).

[16] K. Uematsu, S. Ohsaka, N. Shinohara, and M. Okumiya, "Grain-Oriented Microstructure of Alumina Ceramics Made through the Injection Molding Process," *J. Am. Ceram. Soc.*,**80**[5] 1313-15 (1997).

[17] O. Guillon, L. Weiler, and J. Rödel, "Anisotropic Microstructural Development During the Constrained Sintering of Dip-Coated Alumina Thin Films," *J. Am. Ceram. Soc.*,**90**[5] 1394-400 (2007).

[18] X. Wang and A. Atkinson, "Microstructure Evolution in Thin Zirconia Films: Experimental Observation and Modelling," *Acta Mater.*,**59**[6] 2514-25 (2011).

[19] E. A. Olevsky, "Theory of Sintering: From Discrete to Continuum," *Mater. Sci. Eng. R-Rep.*,**23**[2] 41-100 (1998).

[20] J. S. Patwardhan and W. R. Cannon, "Factors Influencing Anisotropic Sintering Shrinkage in Tape-cast Alumina: Effect of Processing Variables," *J. Am. Ceram. Soc.*,**89**[10] 3019-26 (2006).

[21] M. I. Zainuddin, S. Tanaka, R. Furushima, and K. Uematsu, "Influence of Particles Packing in Granules on the Particles Orientation in Compacts," *J. Eur. Ceram. Soc.*,**31**[1-2] 3-11 (2011).

[22] A. Dellert, A. Heunisch, and A. Roosen, "The Origin of Anisotropic Shrinkage in Tape-cast Green Tapes," *Int. J. Appl. Ceram. Technol.*,**8**[6] 1312-19 (2011).

[23] G. Besendörfer and A. Roosen, "Particle Shape and Size Effects on Anisotropic Shrinkage in Tape-cast Ceramic Layers," *J. Am. Ceram. Soc.*,**91**[8] 2514-20 (2008).

[24] J.-B. Ollagnier, O. Guillon, and J. Rödel, "Effect of Anisotropic Microstructure on the Viscous Properties of an LTCC Material," *J. Am. Ceram. Soc.*,**90**[12] 3846-51 (2007).

[25] R. Mücke, N. H. Menzler, H. P. Buchkremer, and D. Stöver, "Cofiring of Thin Zirconia Films During Sofc Manufacturing," *J. Am. Ceram. Soc.*,**92** S95-S102 (2009).

[26] J.-S. Kim, R. A. Rudkin, X. Wang, and A. Atkinson, "Constrained Sintering Kinetics of 3YSZ Films," *J. Eur. Ceram. Soc.*,**31**[13] 2231-39 (2011).

[27] D. W. Ni, E. Olevsky, V. Esposito, T. T. Molla, S. P. V. Foghmoes, R. Bjørk, H. L. Frandsen, E. Aleksandrova, and N. Pryds, "Sintering of Multilayered Porous Structures: Part

II–Experiments and Model Applications," *J. Am. Ceram. Soc.,* (2013). Doi: 10.1111/Jace.12374

[28] Z. Fu and A. Roosen, "Shrinkage of Tape Cast Products During Binder Burnout," *J. Am. Ceram. Soc.*,**98**[1] 20-29 (2015).

[29] F. Jones and J. Irvine, "Preparation of thin films using the tape-casting process for use in the solid oxide fuel cell," *Ionics*,**8**[5] 339-43 (2002).

[30] W. R. Cannon and P. M. Raj, "Evolution of Sintering Anisotropy Using a 2D Finite Difference Method," *J. Am. Ceram. Soc.*,**92**[7] 1391-95 (2009).

[31] P. M. Raj, A. Odulena, and W. R. Cannon, "Anisotropic Shrinkage During Sintering of Particle-oriented Systems—Numerical Simulation and Experimental Studies," *Acta Mater.*,**50**[10] 2559-70 (2002).

[32] L. Amaral, C. Jamin, A. M. R. Senos, P. M. Vilarinho, andO. Guillon, "Constrained sintering of BaLa4Ti4O15 thick films: Pore and grain anisotropy," *J. Eur. Ceram. Soc.*,**33**[10] 1801-08 (2013).

[33] M. Albano, L. Garrido, K. Plucknett, and L. Genova, "Influence of Starch Content and Sintering Temperature on the Microstructure of Porous Yttria-stabilized Zirconia Tapes," *J. Mater. Sci.*,**44**[10] 2581-89 (2009).

[34] R. Zuo, E. Aulbach, R. K. Bordia, and J. Rödel, "Critical Evaluation of Hot Forging Experiments: Case Study in Alumina," *J. Am. Ceram. Soc.*,**86**[7] 1099-105 (2003).

[35] A. Shui, Z. Kato, S. Tanaka, N. Uchida, and K. Uematsu, "Sintering Deformation Caused by Particle Orientation in Uniaxially and Isostatically Pressed Alumina Compacts," *J. Eur. Ceram. Soc.*,**22**[3] 311-16 (2002).

[36] Y. Zhao and L. R. Dharani, "Theoretical-Model for the Analysis of a Ceramic Thin-Film Sintering on a Non-Sintering Substrate," *Thin Solid Films*,**245**[1-2] 109-14 (1994).

[37] H. L. Zhang, J. F. Li, and B. P. Zhang, "Microstructure and Electrical Properties of Porous Pzt Ceramics Derived From Different Pore-forming Agents," *Acta Mater.*,**55**[1] 171-81 (2007).

[38] C. L. Martin, H. Camacho-Montes, L. Olmos, D. Bouvard, and R. K. Bordia, "Evolution of Defects During Sintering: Discrete Element Simulations," *J. Am. Ceram. Soc.*,**92**[7] 1435-41 (2009).

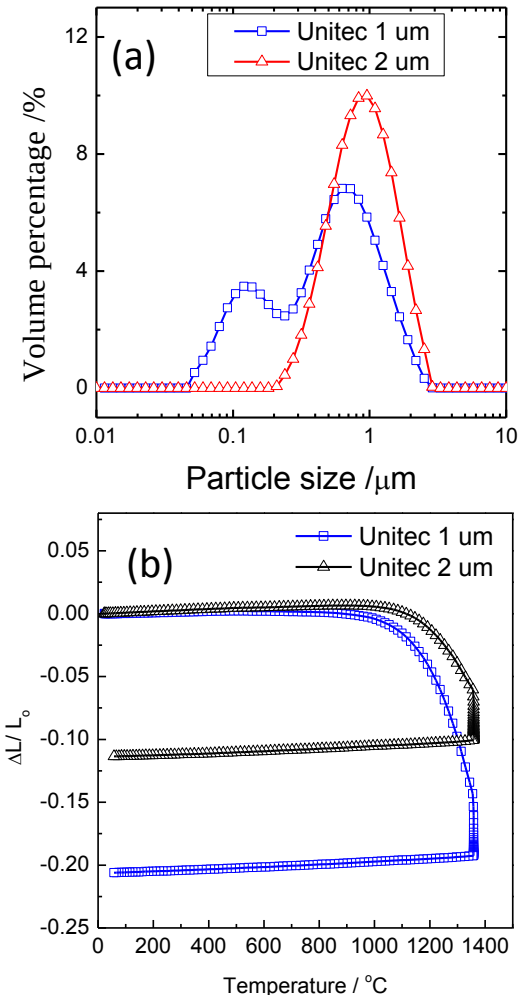

Figure 1. (a) Particle size analysis of the Unitec 1-um and 2-um powder after ball milling for 24 h in isopropanol containing 2 wt.% triton. (b) Dilatometry of the pellets from two powders pressed under 149 MP

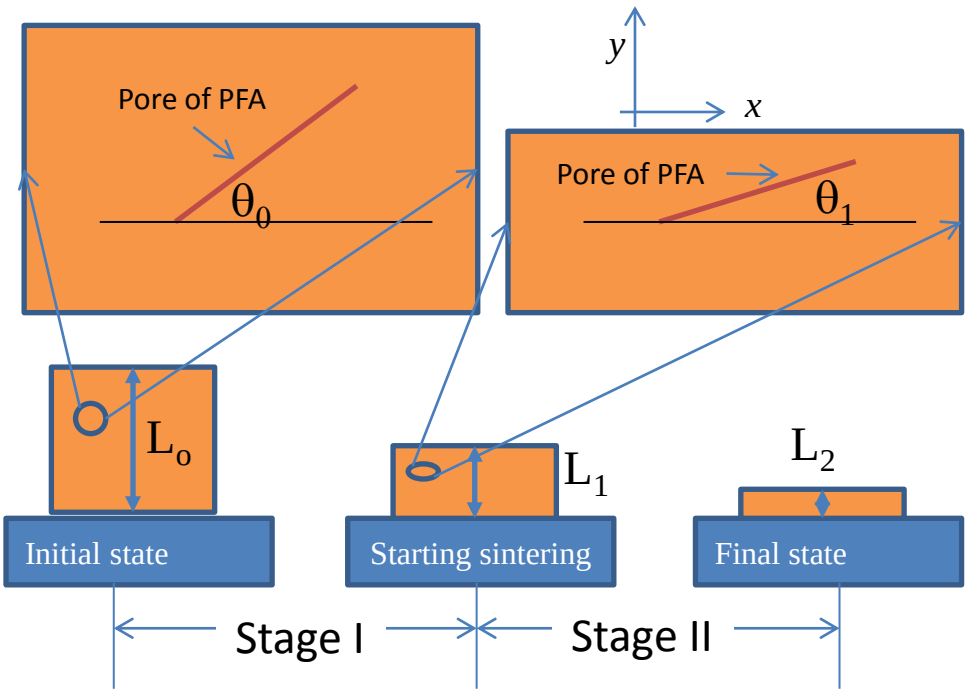

Figure 2. Schematics of the thickness of the deposited film and the orientation of the pore/PFA at different stages. The axes are shown in the image to in indicate x- and y-direction. X-axis is the reference axis for the angle of particles

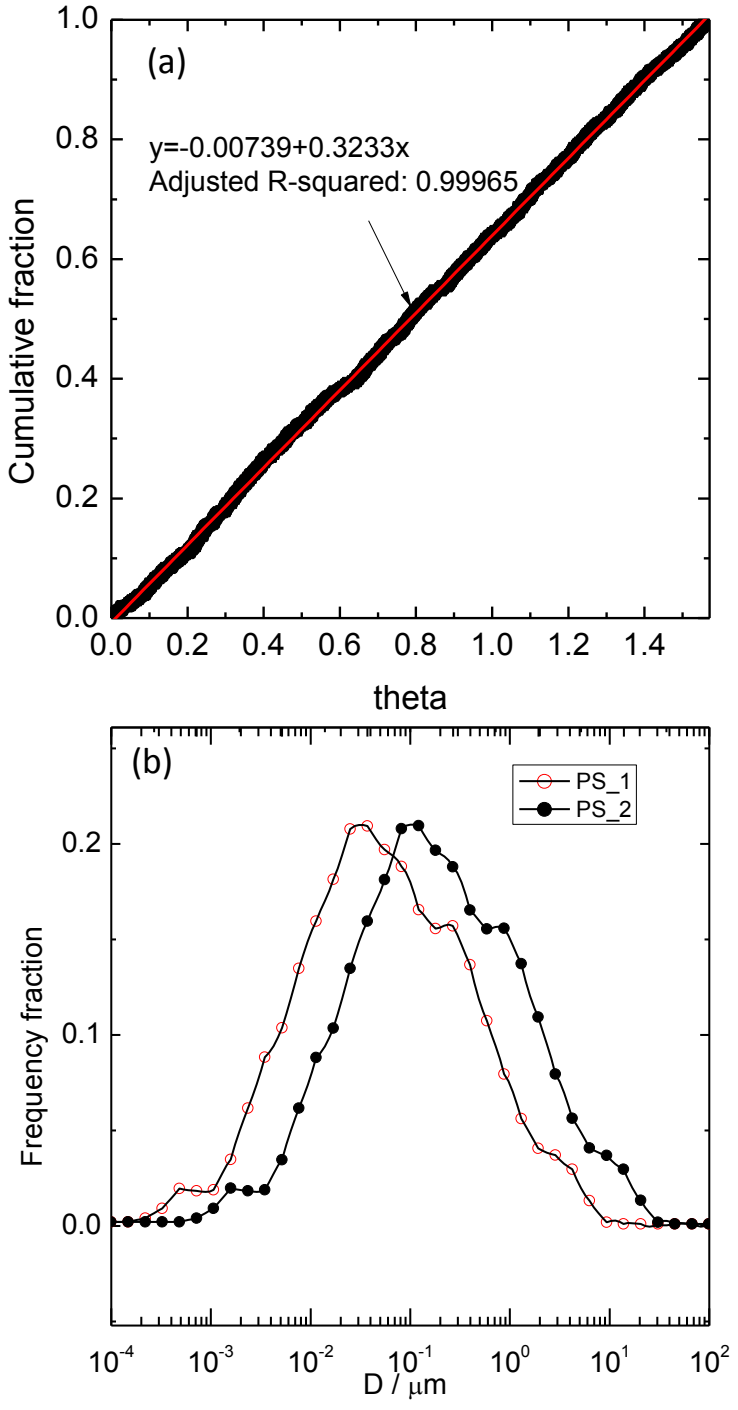

Figure 3 (a) Cumulative angle distribution of the particles in the simulation work; (b) discrete particle size fraction of the 2D pores/PFAs used in the modelling, PS_2 is 4 times larger than PS_1.

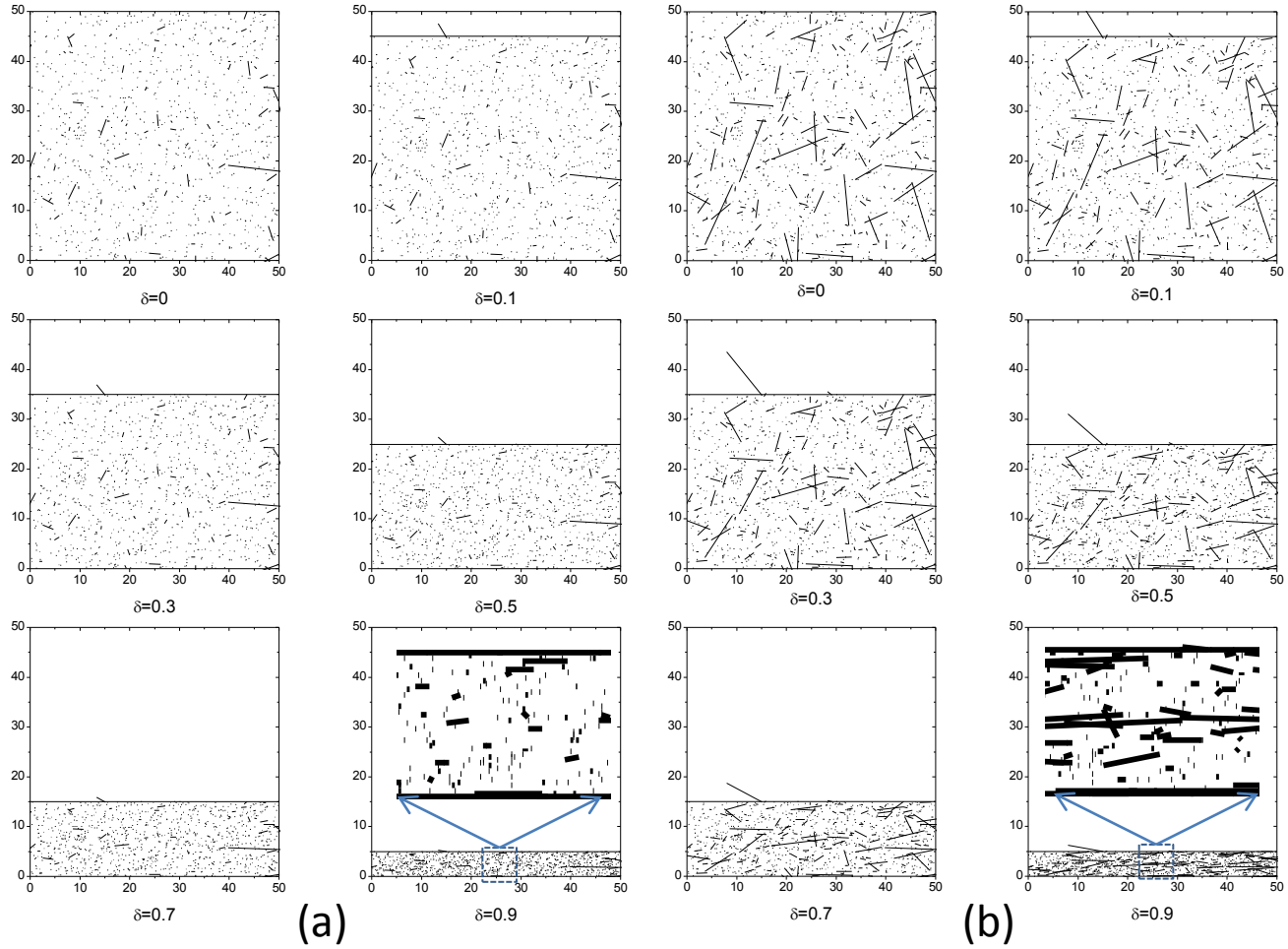

Figure 4. Image evolution with pores/PFAs of random angle distribution at different shrinkage values. The length of the pore/PFAs in figure (a) and (b) is PS_1 and PS_2, respectively. The size of the original image when δ=0 is 50μm x 50 μm. The width of images for the simulation of shrinkage, the width of image is 50 μm and the height change to (1-δ) x 50 μm by pressing the image from the top to the bottom. The insert image when d=0.9 are the zoom-ins of the area in the ellipses.

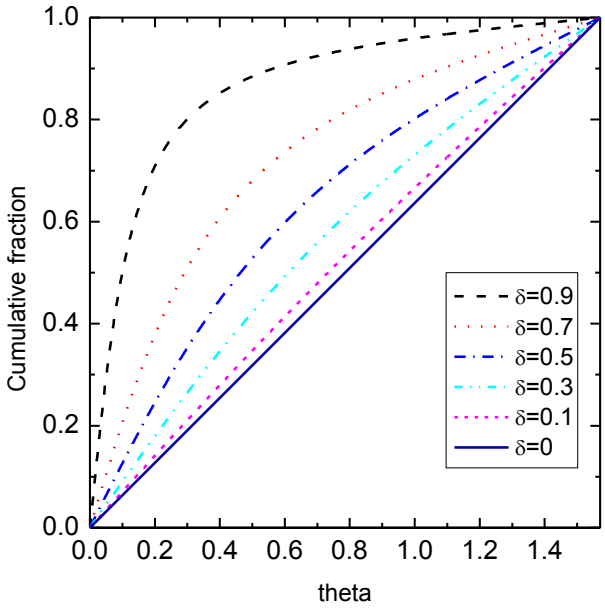

Figure 5. statistics of the angle of the particles at different shrinkage in terms of δ values.

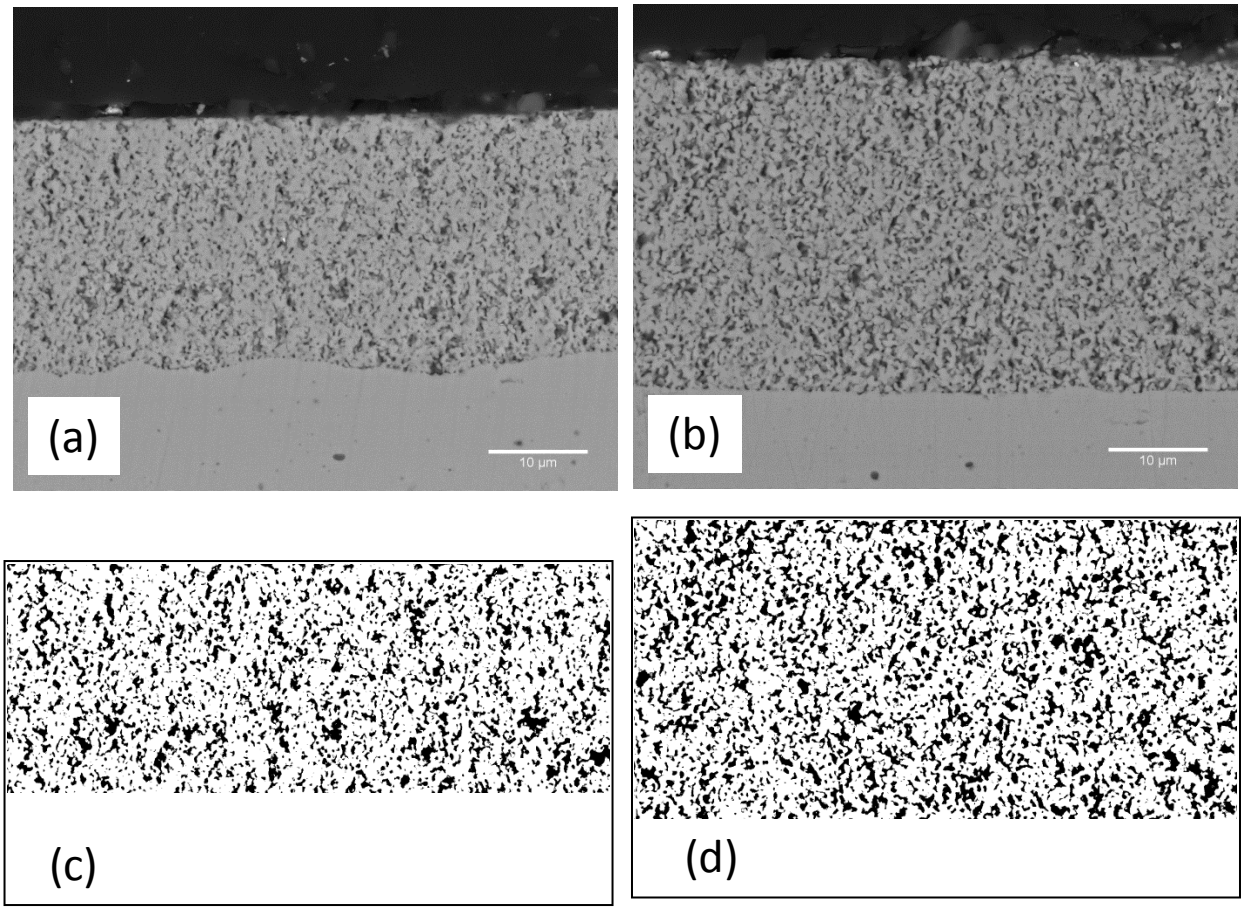

Figure 6. Back-scattered images of the film sintered at 1320 ^{o}C with ink containing Unitec 1 um (a) and 2 um (b) YSZ powder: (c) and (d) is the respective binarized image for calculation of porosity, pore orientation and pore size.

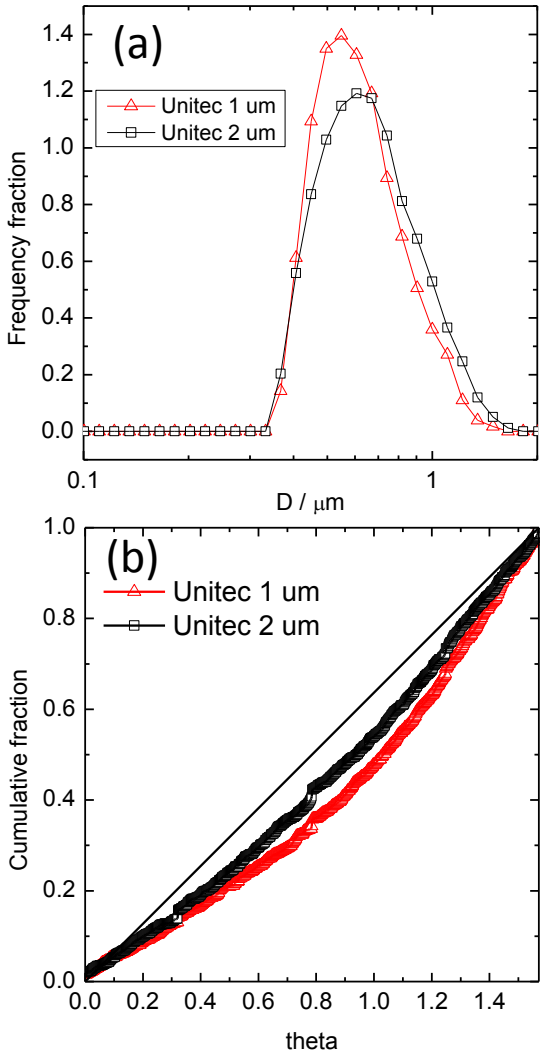

Figure 7. Pore size distribution (a) and cumulative fraction (b) of the constrained film from Unitec 1-um and 2-um YSZ powder.

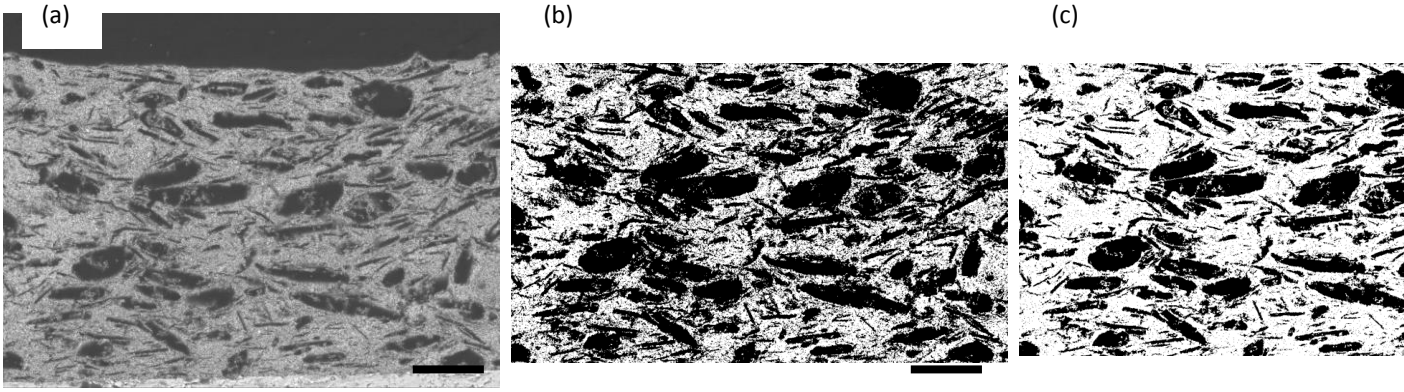

Figure 8. (a) back-scattered image of the film sintered at 1100 ^{o}C with the ink containing YSZ and graphite; (b) binarized image for measurement of pority and (c) despeckled image for measurement of pore size and orientation. The scale bars represent 20 μm.

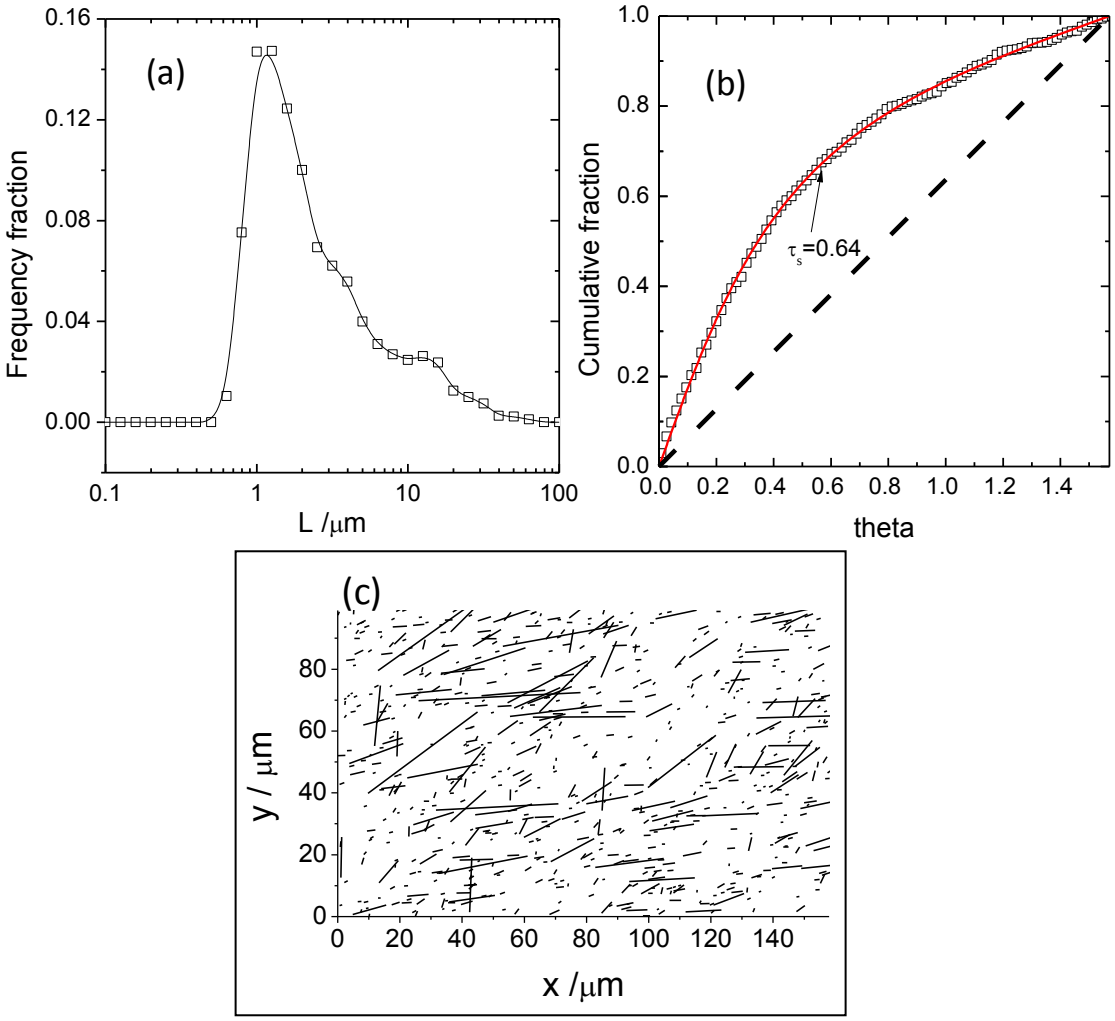

Figure 9. (a) Pore size distribution and (b) cumulative fraction of the pores at different angle. The line in (c) shows an image with the length profile shown in (a) using the angle distribution when τ_s is 0.64.

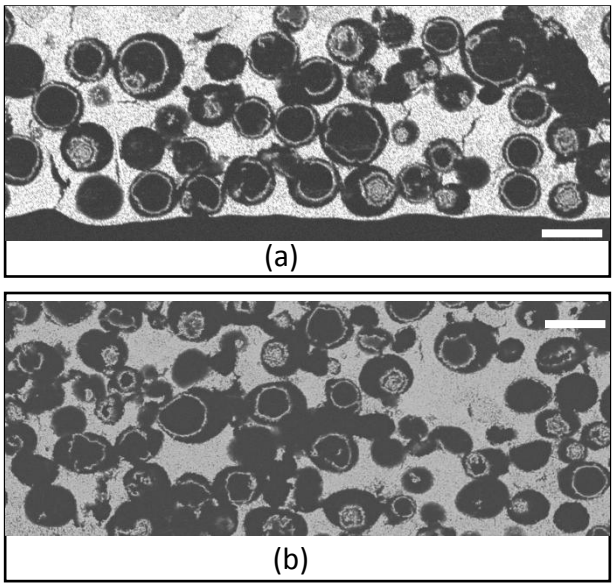

Figure 10. Back-scattered images of the film sintered at 1100 ^{o}C (a) and 1300 ^{o}C (b) from the ink containing YSZ and glassy carbon. The length of scale bar is 20 μm.

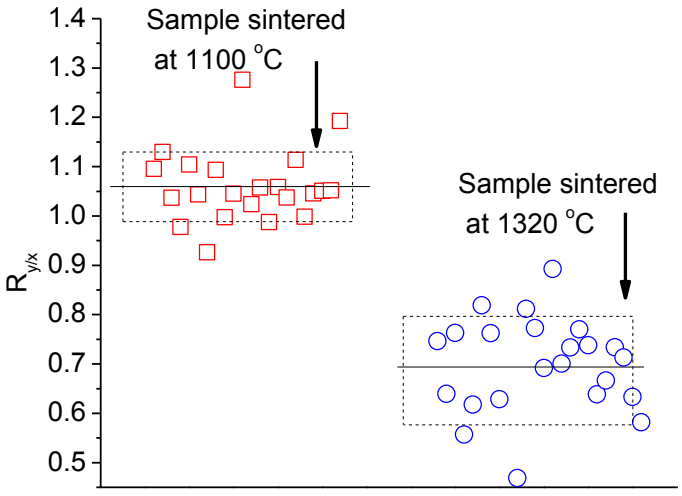

Figure 11 the $R_{y/x}$ values for the pores from glassy carbon after a sintering at 1100 °C and 1320 °C. The straight line in each group of data shows the average value and the rectangle shows the standard deviation.

Table 1. Recipes of the inks with and without pore forming agent (PFA)

No.	ceramic	PFA	vehicle	KD-1	vol.% of ceramic[a]/ V_c	vol.% of PFA[b]/ V_p
1	Unitec 1 um 20.0 g	-	7.80 mL	0.40 g	30.0%	-
2	Unitec 2 um 20.0 g	-	7.80 mL	0.40 g	30.0%	-
3	Unitec 1 um 5.0 g	graphite 1.0 g	4.18 mL	0.12 g	15.0%	9.0%
4	Unitec 1 um 5.0 g	glassy carbon 1.0 g	4.18 mL	0.12 g	14.6%	11.7%

[a]: density of YSZ 6.0 g/cm^3

[b]: gaphite 2.0 g/cm^3 and glassy carbon 1.5g/cm^3

Image analysis and modelling of the orientation of pores in a constrained film on a rigid substrate

*By C.S. Ni & John T.S. Irvine**
Corresponding author: email jtsi@st-andrews.ac.uk

School of Chemistry, University of St Andrews, Fife KY16 9ST, Scotland

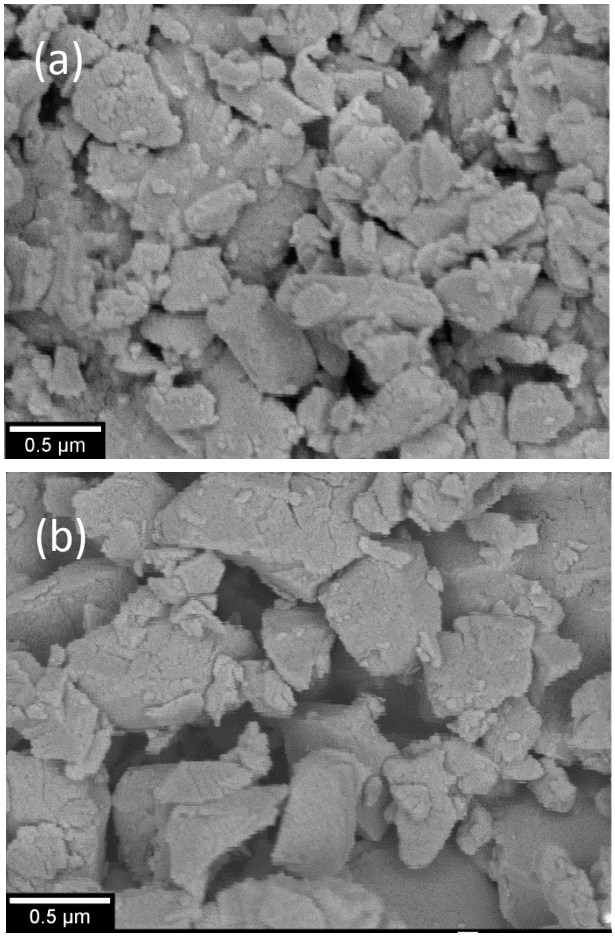

Figure S1. SEM images of the as-received YSZ powders : (a) Unitec 1-um powder and (b) Unitec 2-um.

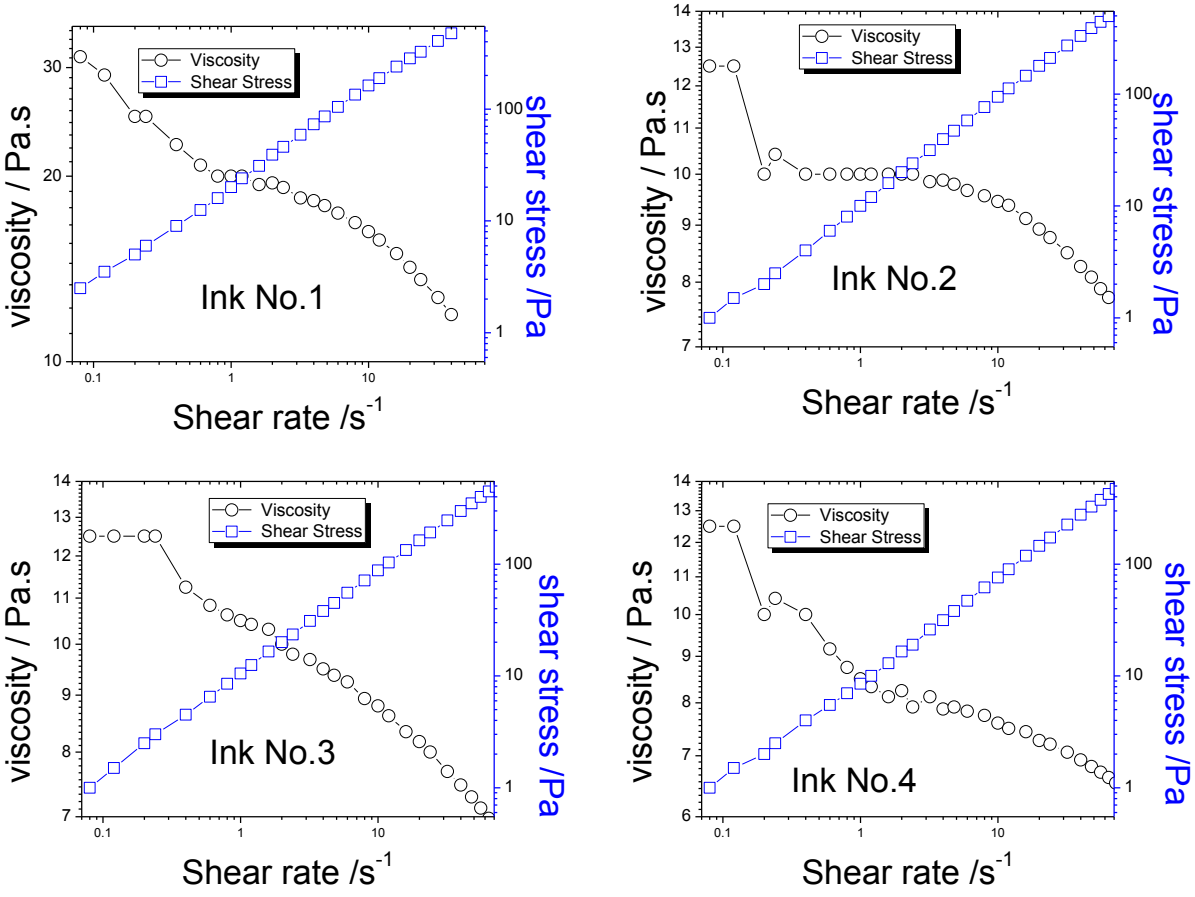

Figure S2. viscosity and shear stress of the four inks collected in the logarithmic mode with increasing shear rate.

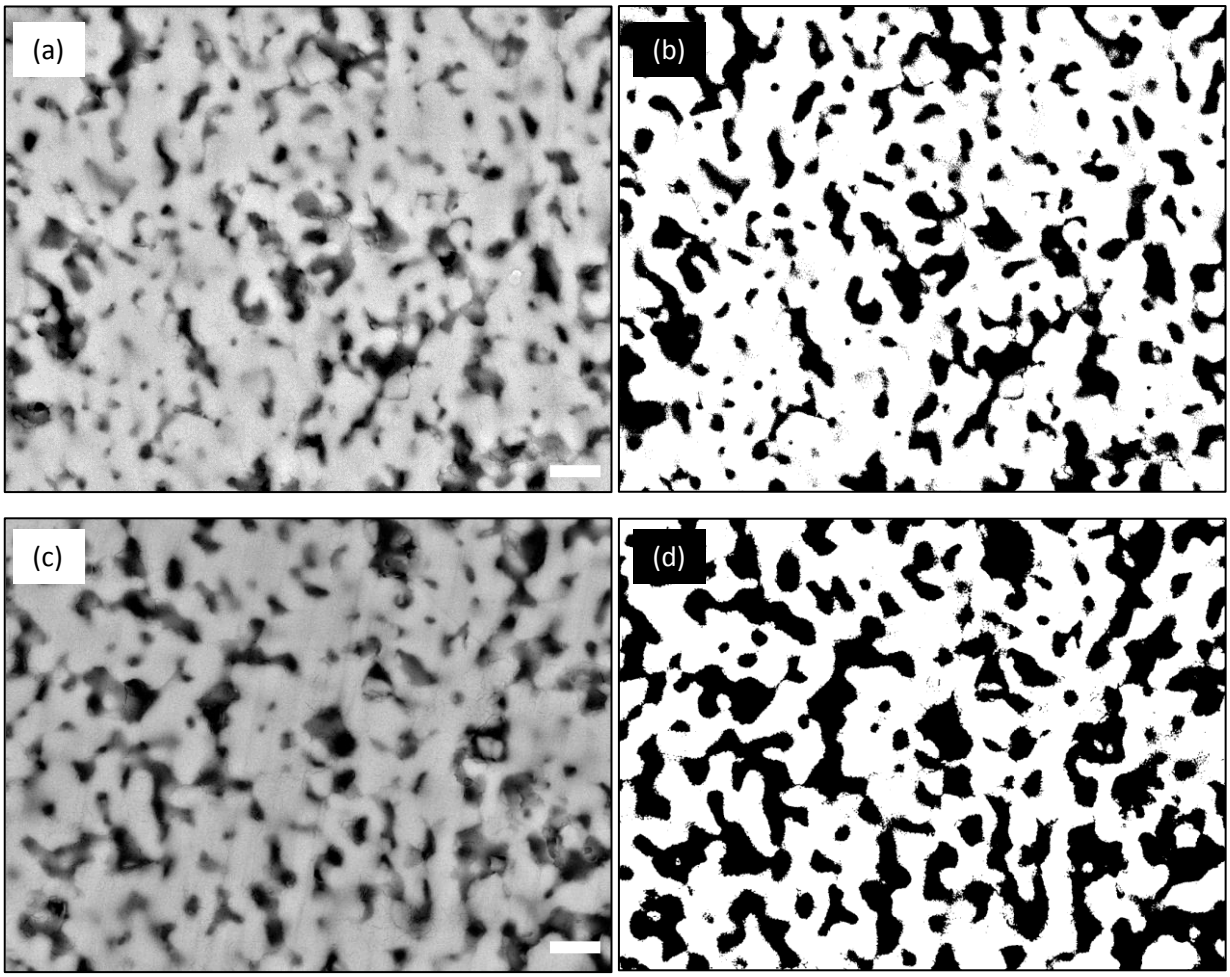

Figure S3. High-magnification images of the film sintered at 1320 ^{o}C with ink containing Unitec 1 um (a) and 2 um (c) YSZ powder: (b) and (d) are the respective binarized image for calculation of porosity.
The porosity from image (b) and (d) is 26.3% and 38.3 % respectively. Five images like this is used for the porosity as stated in the text. The scale bar is 1 μm.